Nanoscale

Accepted Manuscript

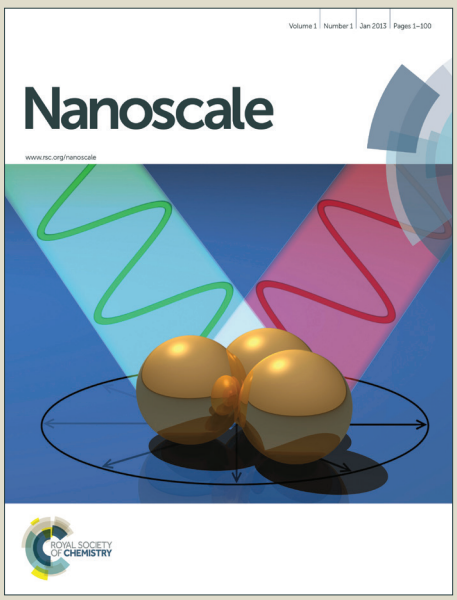

ROYAL SOCIETY OF CHEMISTRY

www.rsc.org/nanoscale

Fluoro-polymer Functionalized Graphene for Flexible Ferroelectric Polymer-based High-*k* Nanocomposites with Suppressed Dielectric Loss and Low Percolation Threshold

Ke Yang[†], Xingyi Huang*[,†], Lijun Fang[†], Jinliang He[‡], and Pingkai Jiang*[,†,§]

[†]Department of Polymer Science and Engineering, Shanghai Key Laboratory of Electrical Insulation and Thermal Aging, Shanghai Jiao Tong University, Shanghai 200240, China

[‡]State Key Lab of Power system, Department of Electrical Engineering, Tsinghua University, Beijing 100084, China

[§]Shanghai Engineering Center for Material Safety of Nuclear Power Equipment, Shanghai 200240, China

Email: xyhuang@sjtu.edu.cn (X. Y. H.), pkjiang@sjtu.edu.cn (P. K. J.)

Abstract:

Flexible nanodielectric materials with high dielectric constant and low dielectric loss have huge potential applications in modern electronic and electric industry. Graphene sheet (GS) and reduced-graphene oxide (RGO) are promising fillers for preparing flexible polymer-based nanodielectric materials because of their unique two-dimension structure and excellent electrical and mechanical properties. However, the easy aggregation of GS/RGO significantly limits the potential of graphene in enhancing the dielectric constant of polymer composites. In addition, the poor filler/matrix nanoscale interfacial adhesion also causes difficulties in suppressing the dielectric loss of the composites. In this work, by using a facile and environmental friendly approach, polydopamine coated RGO (PDA-RGO) and fluoro-polymer functionalized RGO (PF-PDA-RGO) were prepared. Compared with the RGO prepared by the conventional methods [*i.e.*, hydrazine reduced-graphene oxide (H-RGO)] and PDA-RGO, the resulting PF-PDA-RGO nanosheets exhibit excellent dispersion in ferroelectric polymer matrix [*i.e.* poly(vinylidene flyoride-co-hexafluroro propylene), P(VDF-HFP)] and strong interfacial adhesion with the matrix, leading to a low percolation threshold ($f_c = 1.06$ vol%) and excellent flexibility for the corresponding nanocomposites. Among the three nanocomposites, the P(VDF-HFP)/PF-PDA-RGO nanocomposites exhibited the optimum performance (*i.e.*,

simultaneously having high dielectric constant and low dielectric loss) . For instance, at 1000 Hz, the P(VDF-HFP) nanocomposite sample with 1.0 vol% PF-PDA-RGO has a dielectric constant of 107.9 and dielectric loss of 0.070, showing good potential for dielectric applications. Our strategy provides a new pathway to prepare high performance flexible nanodielectric materials.

Key words: graphene, reduced-graphene oxide (RGO), dielectric materials, interface, polymer nanocomposites, dopamine

Introduction

Flexible dielectric materials with high dielectric constant and low dielectric loss play an important role in deriving the continuing development of high performance electronic devices such as embedded capacitors, organic field-effect transistors (OFETs) and electroactive actuators.[1-3] Recent advances have revealed that an effective way to enhance the high dielectric constant while preserving the low dielectric loss of dielectric polymer is to introduce high dielectric constant ceramic fillers.[4-13] However, a relatively high loading of ceramic filler (>50 vol%) is often needed to realize a high enough dielectric constant because of the large dielectric constant difference between the filler and matrix, which inevitably raises the issues of inhomogeneity and aggregation filler in the polymer matrix, resulting in many shortcomings such as poor mechanical properties, low flexibility and high density.[14-20] To overcome these disadvantages, a promising strategy for flexible nanodielectrics has been developed by constructing percolative systems, namely, preparing composites by introducing conductive fillers (eg., metal nanoparticles, carbon black and carbon nanotubes) into polymer matrices.[21-24] By using these methods, a very high dielectric constant can be achieved at a low volume fraction of fillers and thus the flexibility of the polymer is usually preserved in the composites.[25]

Owing to their excellent electrical, thermal, optical and mechanical properties, graphene sheet (GS) and reduced-graphene oxide (RGO) have been widely used as fillers to enhance the performances of polymers.[26-28] Additionally, GS/RGO are 2-D thin films with thickness in sub-nanometer and width in several to tens micrometer, which make them easily be connected into 3-D network structures in a polymer matrix.[29-32] In this case, they are very promising candidates as conductive fillers to prepare highly flexible nanodielectrics by constructing

percolative systems.[33-38] For example, Jiang et al prepared poly(vinylidene fluoride) (PVDF)/GS nanocomposite films by solution blending. The authors found that the incorporation of GS simultaneously increased the dielectric properties and thermal properties of PVDF, resulting in a high dielectric constant of 30 at 1000 Hz near the percolation threshold of 3.6 vol% and over 20 ℃ increase of the maximum decomposition temperature of PVDF.[39] Sodano et al. used monolayer RGO as fillers to prepare PVDF nanocomposites.[40] It is found that the dielectric constant of the PVDF/RGO nanocomposites was significantly enhanced to 100 near the percolation threshold (*i.e.*, 1.6 vol%), which is 10 times larger than that of pure PVDF. Although relatively high dielectric constant was obtained, the dielectric loss of the PVDF/RGO and PVDF/GS nanocomposites is still high. In addition, it is believed that the full potential of graphene was not realized in enhancing the dielectric constant of the nanocomposites.

To solve aforementioned problems, significant efforts have been devoted to prepare polymer functionalized GS/RGO.[41-43] In this strategy, the polymers are grafted or attached onto the surfaces or edges of GS/RGO, not only acting as the interlayers to prevent the agglomeration of the fillers, but also enhancing the compatibility between the fillers and polymer matrix. Nevertheless, these methods also suffer from some drawbacks. For example, some hazardous reagents are usually used in the process of functionalization and chemical reduction, which are difficult to be removed completely,[44, 45] leading to high dielectric loss and high leakage current in the corresponding nanocomposites. Consequently, it is highly necessary to develop other facile and environmental friendly approaches to prepare polymer functionalized GS/RGO for polymer nanocomposite dielectrics.

It has been found previously that dopamine (DA), a mussel inspired molecule, could undergo self-polymerization to produce an adherent polydopamine (PDA) coating on almost any solid surface in a weak alkaline aqueous solution.[46, 47] After the self-polymerization, the catechol groups of DA will be oxidized to quinone form, which can act as the anchor to graft other functional molecules or polymers via the thiol, amine, and imino groups, Michael addition or Schiff base reactions.[47-49] In addition, DA is also an effective reducing agent, which can convert GO into chemically reduced RGO via an environmental friendly route.[49-52] More importantly, PDA is a semiconductor, which can repair the defects of RGO and enhance their electrical conductivity by π-π stacking.[29, 53] Therefore, DA has been widely used to prepare functionalized

RGO for biomedical, environmental and energy applications.[54, 55]

In this study, we developed a facile and environmental friendly approach to prepare fluoro-polymer functionalized RGO for flexible ferroelectric polymer-based nanocomposite dielectrics. In this method, GO was simultaneously reduced and functionalized by DA without using any hazardous reagents, resulting in uniform and well dispersed PDA coated RGO (PDA-RGO). The final functionalization was finished by grafting thiol-terminated poly(trifluoroethyl acrylate) onto the surfaces of PDA-RGO through Michael addition. The fluoro-polymer functionalized RGO (PF-PDA-RGO) was used as the conductive filler to prepare P(VDF-HFP)-based nanodielectrics by solution blending and hot compression molding. The surface-grafted fluoro-polymer used in this work has similar chemical structure and surface energy with P(VDF-HFP) matrix, which not only can improve the dispersion of RGO but also can enhance the interfacial adhesion between the fillers and fluoro-polymer matrix. Our results show that the highly flexible ferroelectric polymer-based nanocomposite dielectrics were successfully prepared, which not only have a relative low percolation threshold, but also exhibit high dielectric constant and low dielectric loss.

Experimental Section

Materials

Graphene oxide (GO) was synthesized from natural graphite powder according to our previous work[56] through the modified Hummers method.[57] Dopamine hydrochloride (DA-HCl, 98%), tris(hydroxymethyl) aminomethane (Tris, 99%), hydrazine hydrate (85%) were purchased from Sigma-Aldrich and used without further purification. Thiol-terminated poly(trifluoroethyl acrylate) (PF-SH, Mn: 6000 g/mol, Mw/Mn = 1.21) was synthesized by RAFT polymerization and subsequent thiol-modification according to the methods described in literature.[58] Poly(vinylidene fluoride-co- hexafluoropylene) (P(VDF-HFP)) with 15% HFP was purchased from Solvay Plastics (Solef® 21216, molecular weight: 570~600 kDa). N,N-Dimethyl formamide (DMF), ethanol, and other organic reagents or solvents were supplied by Shanghai Reagents Co. Ltd.

Preparation of hydrazine reduced graphene oxide (H-RGO)

The hydrazine reduced graphene oxide was prepared as the follows: 100 mg GO was dispersed in 500 mL aqueous solution followed by sonication for 30 min in an ice bath; then 0.5 mL hydrazine hydrate was added and the mixture was stirred vigorously at 95 ℃ for 2 h, and then the solution was filtered with a 0.2 μm membrane filter, washed and redispersed with deionized water, followed by dialysis in deionized water for 48 h. The H-RGO was obtained as a black power by filtration and dried under reduced pressure at 60 ℃ for 24 h.

Preparation of polydopamine-coated reduced graphene oxide (PDA-RGO)

PDA-RGO was synthesized according to the literature method.[49, 51] 100 mg GO was dispersed in 500 mL 10 mM Tris-HCl aqueous solution (pH 8.5) followed by sonication for 30 min in an ice bath; then 200 mg DA-HCl was added and sonicated for another 10 min. The mixture was stirred vigorously at 70 ℃ for 24 h, and then the solution was filtered with a 0.2 μm membrane filter, washed and redispersed with deionized water, followed by dialysis in deionized water for 48 h. The PDA-RGO was obtained as a black power by filtration and dried under reduced pressure at 60 ℃ for 24 h.

Preparation of fluoro-polymer functionalized RGO (PF-PDA-RGO)

PF-PDA-RGO was prepared as the follows: 100 mg PDA-RGO was re-dispersed into 300 mL ethanol solution followed by sonication for 15 min in an ice bath; then 100 mL DMF solution containing 400 mg PF-SH was added and sonicated for another 10 min. The mixture was stirred vigorously and the graftiong reaction was carried out at 25 ℃ for 24 h, and then the solution was centrifuged at 10 000 rpm for 20 min. The product was redispersed in ethanol, and the mixture was centrifuged; this cycle was repeated three times to remove the un-grafted PF. The PF-PDA-RGO was obtained as a black power after drying the product under reduced pressure at 60 ℃ for 24 h.

Preparation of P(VDF-HFP)-based nanocomposites

The typical procedures for the preparation of P(VDF-HFP)/PF-PDA-RGO nanocomposites were carried out as follows: A certain amount of P(VDF-HFP) was first dissolved in DMF and stirred for 1 h at 60 ℃. At the same time, a desired amount of PF-PDA-RGO was also dispersed in 10 mL DMF by sonication for 5 min. Then, the two solutions were mixed slowly and stirred at room temperature for 12 h. Upon completion, the mixture was casted onto a glass plate and dried in an oven for 2 h at 90 ℃. The obtained films were collected and dried under reduced pressure at

60 ℃ for 24 h in order to remove the remaining trace of solvent. And then, the nanocomposite films for testing were prepared by hot compression molding at 180 ℃. The typical thickness of the films in this work is around 40-50 μm.

The procedures for the preparation of P(VDF-HFP)/PDA-RGO nanocomposites and P(VDF-HFP)/H-RGO nanocomposites were the same as described above, except for using PDA-RGO and H-RGO, respectively.

Characterization

The chemical structures of the functionalized RGO were characterized by Fourier-transform infrared (FT-IR) spectrum with a Paragon 1000 (Perkin-Elmer) spectrometer, and the X-ray photoelectron spectroscopy (XPS) of the samples were also recorded using an Axis Ultra spectrometer (Kratos Analytical, UK) with a monochromated Al Kα source. The morphology and microstructure of the samples were investigated by TEM (JEM-2010, JEOL, Japan), energy-dispersive X-ray (EDX) (Link-Inca, model 622, U.K.), AFM (IMODE NANOSCOPE, DI, USA), XRD (D/max-2200/PC, Rigaku, Japan), and Raman spectroscopy (LabRam HR800, Jobin Yvon, France). Thermo gravimetric analysis (TGA) was conducted by a NETZSCH TG209 F3 instrument with a heating rate of 20 ℃ min^{-1} in a nitrogen flow (20 mL min^{-1}). Differential scanning calorimetry (DSC) measurements were conducted in a NETZSCH 200 F3 instrument at temperatures between 20 and 200 ℃ and a heating/cooling rate of 10 ℃ min^{-1} under a nitrogen atmosphere (the flow rate of purge gas is 20 mL min^{-1}). Scanning electron microscopy (SEM) images of the P(VDF-HFP)-based nanocomposites were taken on a field-emission SEM (JSM-7401F, JEOL, Japan) at an acceleration voltage of 5 kV, All samples were prepared by fracturing the composites at liquid nitrogen temperature and then sputter-coated with a homogeneous gold layer to avoid accumulation of charges. A Novocontrol Alpha-N high resolution Dielectric Analyzer (GmbH Concept 40) was used to measure the dielectric properties of the samples. All the measurements were carried out in the frequency range from 10^{-1} to 10^{7} Hz at room temperature, applying 1.0 ac voltage across two opposite sides of the disk-shaped samples and a layer of gold was evaporated on both surfaces to serve as electrodes, the actual electrode size of our samples is 10 mm in diameter.

Results and discussion

Preparation and characterization of functionalized RGO

It is well-known that the chemically derived GO sheets are heavily oxygenated, bearing hydroxyl, carbonyl and epoxide functional groups on their basal planes and edges,[59] which cause non-conjugated structure and defects in GO and thus deteriorated electrical and thermal properties. To reduce the GO and simultaneously repair the defects, dopamine (DA) as an effective reducing agent was chosen in this study. As described in Scheme 1, the PDA-RGO was prepared via the simultaneous reduction of GO by DA and self-polymerization of the latter. Then, the thiol-terminated poly(trifluoroethyl acrylate) (PF-SH) chains were grafted onto the PDA-RGO via Michael addition, which can prevent the aggregation of RGO sheets and improve the compatibility between the RGO and P(VDF-HFP) matrix. For comparison, the hydrazine reduced GO (H-RGO) without further functionalization was also prepared (Scheme 1). It is found that, similar to GO, PDA-RGO and PF-PDA-RGO can be stably dispersed in dimethylformamide (DMF) more than 72 h after sonification, whereas H-RGO was prone to aggregate in DMF (Fig. S1, ESI).

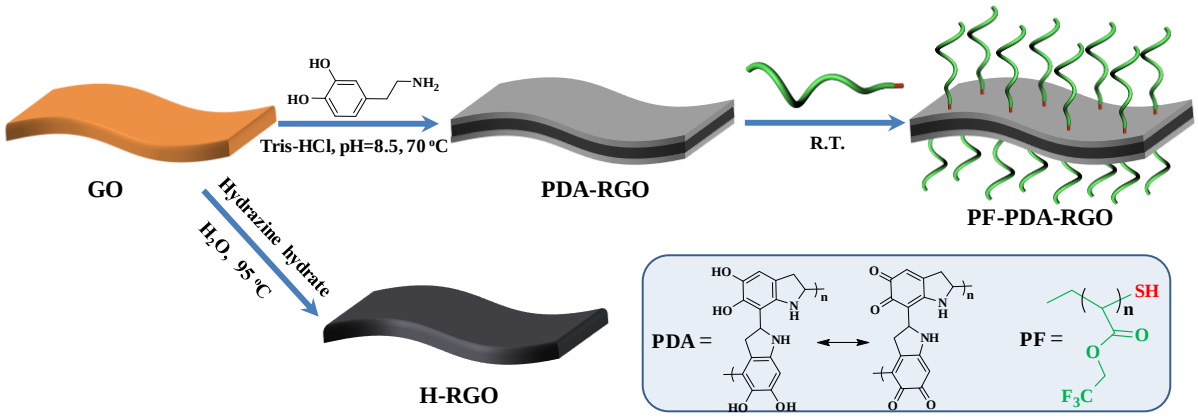

Scheme 1. Schematic illustration for the preparation of H-RGO, PDA-RGO and PF-PDA-RGO.

The chemical structures of the GO and RGO were firstly characterized by FT-IR spectra (Fig. 1A). Compared with the pristine GO, the absence of absorption bands at 1000-1280 cm^{-1} (–C–O and –C–O–C–), 1380 cm^{-1} (–C–OH), and 2800-3000 cm^{-1} ($–CH_2$, $–CH_3$) in H-RGO revealed that most hydroxyl, carbonyl and epoxide functional groups were removed during the reduction process. For PDA-RGO, the absorption bands at 2800-3000 cm^{-1} ($–CH_2$, $–CH_3$), the peak at 1745

cm^{-1} (–C=O in quinone), and the absorption bands at 1100-1250 cm^{-1} (–C–N in secondary amine) are observed and the absorption bands at 3000-3700 cm^{-1} (–OH and –N–H) become stronger, indicating that PDA has been successfully coated onto the graphene backbone.[51] After the grafting of PF, the FT-IR spectrum of PF-PDA-RGO shows the characteristic absorption peaks at 1100-1200 cm^{-1} and 1400 cm^{-1} (–C–F strecthing).[20] Additionally, the absorption bands at 2800-3000 cm^{-1} ($–CH_2$, $–CH_3$) become stronger than that of PDA-RGO. These results indicate that the fluoro-polymer functionalized RGO was successfully prepared.

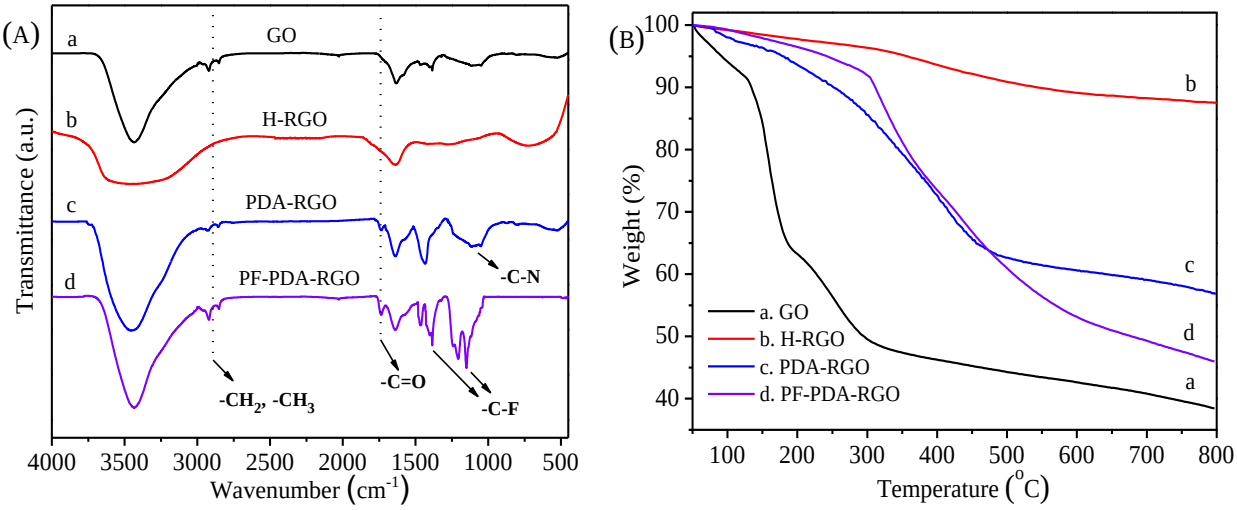

Fig. 1 (A) FT-IR spectra and (B) TGA curves of GO, H-RGO, PDA-RGO and PF-PDA-RGO.

TGA was used as a complementary technique for investigating the composition and thermal stability behaviors of the GO, H-RGO, PDA-RGO and PF-PDA-RGO. It is observed from Fig. 1B that GO shows multiple weight loss processes in the range of 50 to 800 ℃ and starts to lose weight upon heating even below 100 ℃, which is attributed to the volatilization of stored water in its π-stacked structure. The major weight loss appears in the range of 140 to 300 ℃, indicating the pyrolysis of labile oxygen-containing groups.[41] And then, the gentle weight loss in the range of 300 to 800 ℃ can be assigned to the decomposition of carbon backbone. Instead, it can be noted that H-RGO is thermally stable and subject to minor weight loss because most of the oxygen-containing groups on the surface of GO were removed in the reduction process. Despite being reduced by dopamine, PDA-RGO shows a large weight loss process in the range of 200 to 450 ℃ (*see* line c in Fig. 1B), which should be attributed to the surface coating of PDA on RGO.[51] Similar to PDA-RGO, PF-PDA-RGO is subject to a major weight loss from 300 ℃,

which should be attributed to the decomposition of PDA and PF (*see* line d in Fig. 1B). Additionally, it is also can be observed that the thermal stability of PF-PDA-RGO was effectively enhanced in comparison with the PDA-RGO after grafting the PF chains, because of the high thermal stability and flame resistance of the fluoro-polymer.[60] Based on the TGA results (Fig. 1B), the weight content of PDA and PF-PDA in PDA-RGO and PF-PDA-RGO were calculated by using the H-RGO as reference. The results reveal that there are 30.69 wt% of PDA in PDA-RGO and 41.54 wt% of PF-PDA in PF-PDA-RGO, respectively. The density of the functionalized RGO nanosheets can also be calculated, which is about 1.92 g/cm^3 for PDA-RGO and 1.84 g/cm^3 for PF-PDA-RGO (the calculation method of density is listed in ESI).

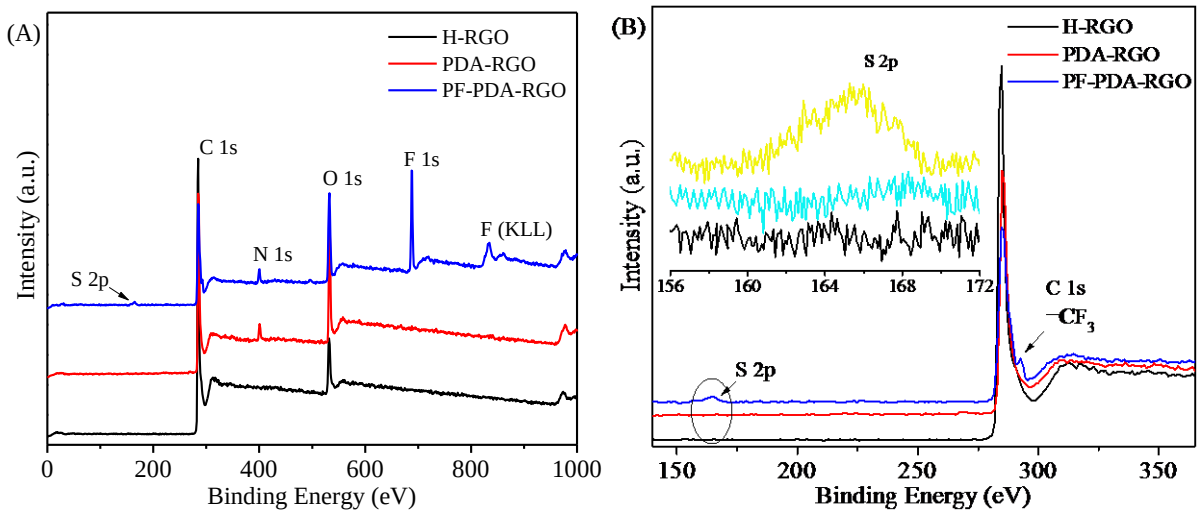

Fig. 2 XPS spectra of H-RGO, PDA-RGO and PF-PDA-RGO, (A) the full spectra and (B) the spectra between 150 to 350 eV. Inset in (B) shows the high-resolution spectra of the S 2p region marked by the cycle.

XPS (Fig. 2) was also employed to investigate the detailed chemical structures of RGO after the functionalization with PDA and PF. Compared with the XPS spectrum of H-RGO, the appearance of N 1s peak at about 400 eV and the enhanced intensity of O 1s peak at about 532 eV in PDA-RGO and PF-PDA-RGO confirm the successful coating of PDA (Fig. 2A).[49] In addition, the appearance of strong F 1s peak at about 687 eV reveals that the PF was successfully grafted onto the PDA-RGO. To gain more clear insights, we provided the XPS spectra between 150 to 350 eV. It can be observed that there are a shoulder peak at 292.6 eV corresponding to C 1s in –CF_3 and a small peak at about 164 eV corresponding to S 2p (Fig. 2B), which further prove the successful preparation of PF-PDA-RGO.[48]

The successful reduction and functionalization of the RGO was further confirmed by XRD and Raman measurements. As shown in Fig. S2A, the XRD pattern of GO exhibits a characteristic peak at 9.8 ° corresponding to a *d*-spacing of 0.91 nm. The appearance of this peak is because of the existence of hydroxyl, carbonyl and epoxide functional groups in GO.[51] When the GO was reduced by hydrazine hydrate, there is no peak at 9.8 ° and a new broad diffraction peak appears at 24.6 ° for H-RGO, suggesting that most of the oxygen-containing groups of GO have been removed and that a fraction of H-RGO sheets were reassembled into the π-stacked structures along the (002) direction without functionalized oxygen-containing groups. A similar phenomenon has been widely observed in recent studies on the reduction of GO.[33, 59] Meanwhile, the stacking peak of PDA-RGO exhibits a lower intensity when compared with H-RGO. For PF-PDA-RGO, the peak intensity further decreases and almost no diffraction peaks can be observed in the testing scope. These results indicate that the typical π-stacked structures of the RGO sheets have been effectively prevented by the PDA coating and PF grafting.

Fig. S2B shows the Raman spectra of the GO and RGO. For the spectrum of GO, two strong peaks are observed around 1345 and 1593 cm^{-1}, which are corresponding to D-band (originating from the disordered carbon atoms) and G-band (originating from the crystalline graphitic carbon atoms), respectively.[26] As for the spectra of H-RGO, PDA-RGO and PF-PDA-RGO, however, the G-band shift to a low-wavelength range, suggesting a significant decrease of oxygen-containing functionalized groups on the graphene backbone. Generally, the peak area ratio of D-band to G-band (I_D/I_G) can give an indication of the defect degree and the surface functionality for the graphene backbone. In this work, the calculated I_D/I_G ratio is 0.98 for GO, which increases to 1.27, 1.21 and 1.22 for H-RGO, PDA-RGO and PF-PDA-RGO, respectively. The increment of the I_D/I_G ratio for RGO and functionalized RGO can be ascribed to the existence of unrepaired defects in graphene backbones after the removal of labile oxygen-containing groups. This phenomenon is similar to the results reported in previous studies on the reduction of GO.[61] In addition, it should be noted that the I_D/I_G ratio of PDA-RGO and PF-PDA-RGO are lower than that of H-RGO, indicating that the backbone of PDA-RGO and PF-PDA-RGO contain a smaller number of defects in comparison with H-RGO.[30]

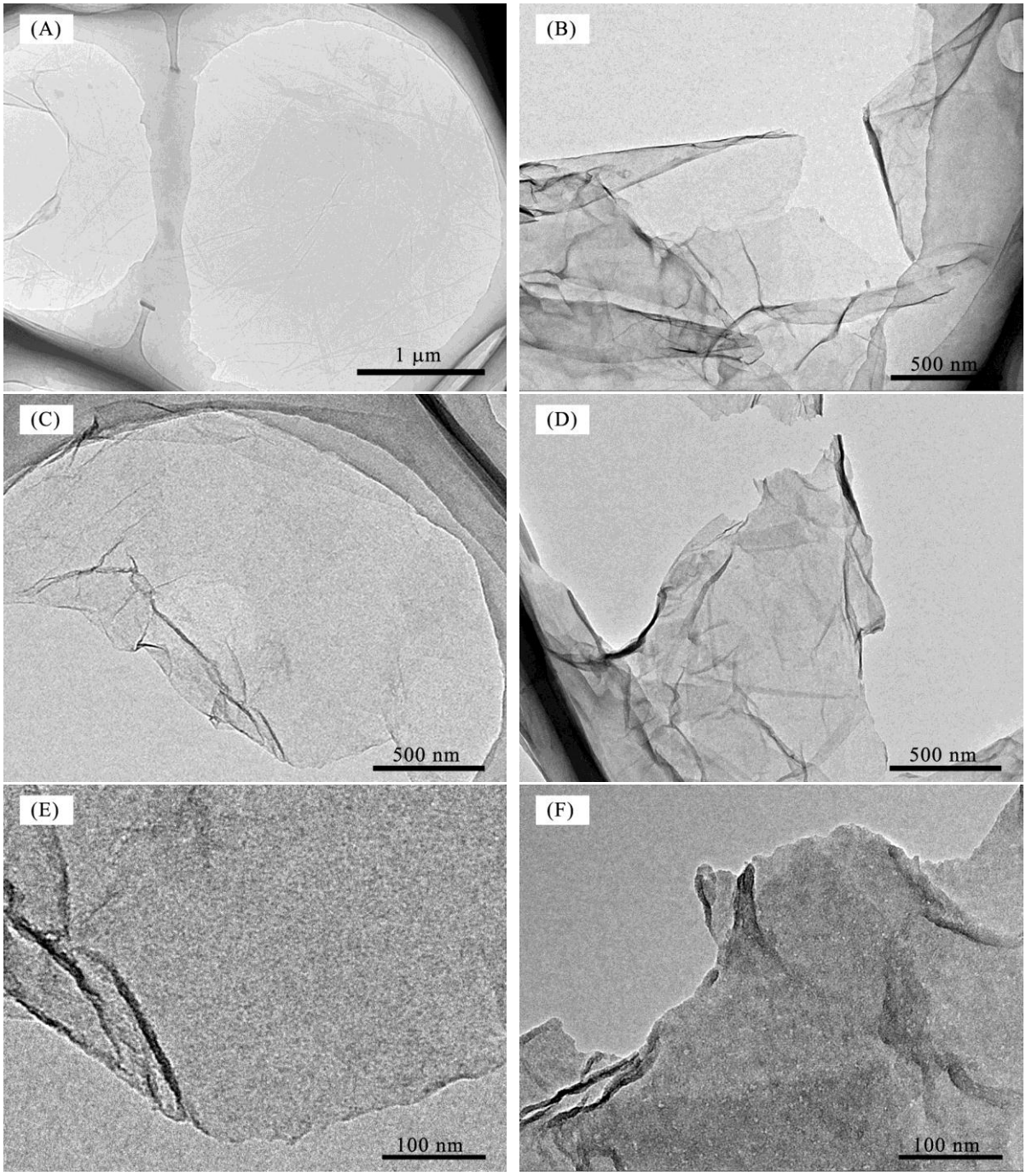

Fig. 3 TEM images of (A) GO, (B) H-RGO, (C) PDA-RGO and (D) PF-PDA-RGO at low magnification; (E) PDA-RGO and (F) PF-PDA-RGO at high magnification.

The morphologies of the GO and surface functionalized RGO were illustrated by TEM. Fig. 3A shows typical wrinkled thin sheets with several micrometers and fairly smooth surface, which are the characteristics of the oxidized exfoliated GO sheets. In contrast, the H-RGO nanosheets are prone to aggregate because of the removal of oxygenated functionalized groups, as shown in Fig. 3B. After being reduced and decorated by PDA, the PDA-RGO sheets maintain the 2-D

nanosheet morphology. When compared with GO and H-RGO, the surface of PDA-RGO appears to be rough and clearly covered by some decorations, which are attributed to the coating of PDA (Fig. 3C and E). As for PF-PDA-RGO, the sheet surface become rougher and more decorations can be observed, indicating the PF was successfully grafted onto the surface of PDA-RGO (Fig. 3D and F). The energy-dispersive X-ray (EDX) analysis provides more direct evidences for the functionalization of RGO by PDA and PF. As shown in Fig. S3 (*see* ESI), apart from copper element from the grid, the EDX pattern of H-RGO only shows carbon and oxygen elements, while the pattern of PDA-RGO appears a new peak of nitrogen element. Meanwhile, the intensity of oxygen element in PDA-RGO is obviously stronger than that of H-RGO because that many oxygen-containing groups were introduced by PDA. After the grafting of PF, a new peak of fluorine appears in the pattern of PF-PDA-RGO. These results are consistent with the XPS results, which further confirm the successful preparation of PDA-RGO and PF-PDA-RGO.

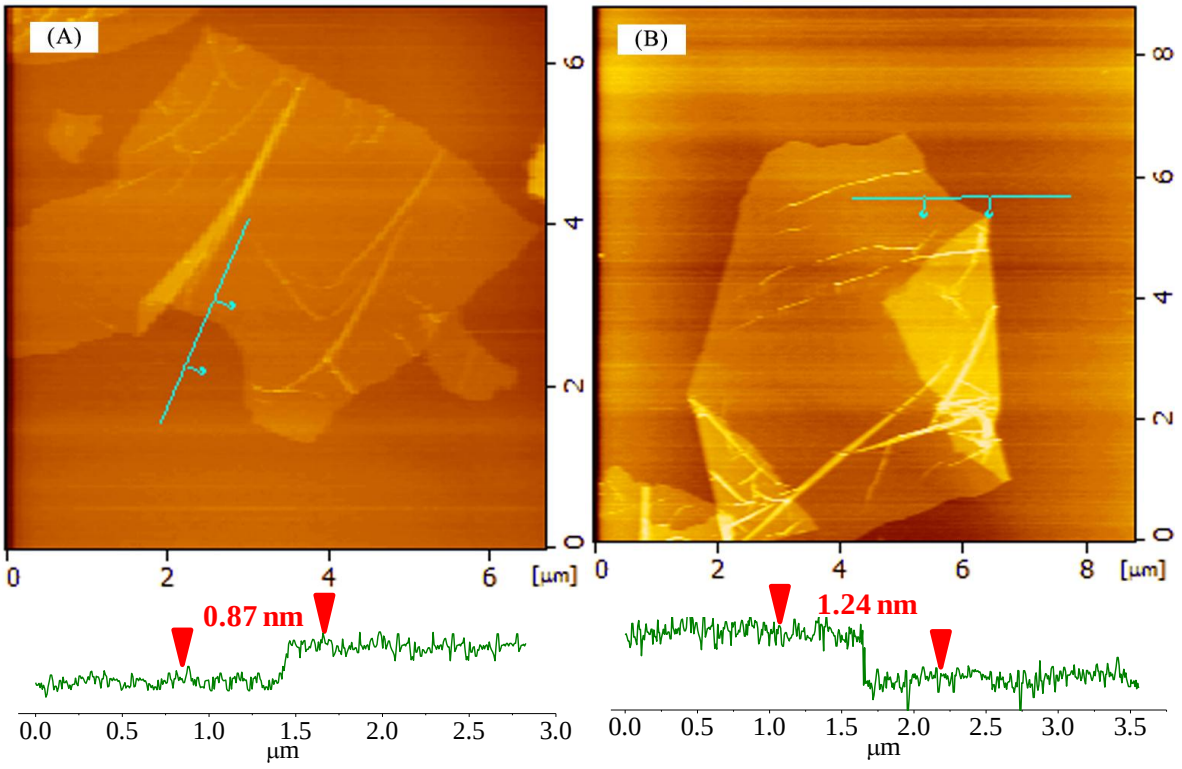

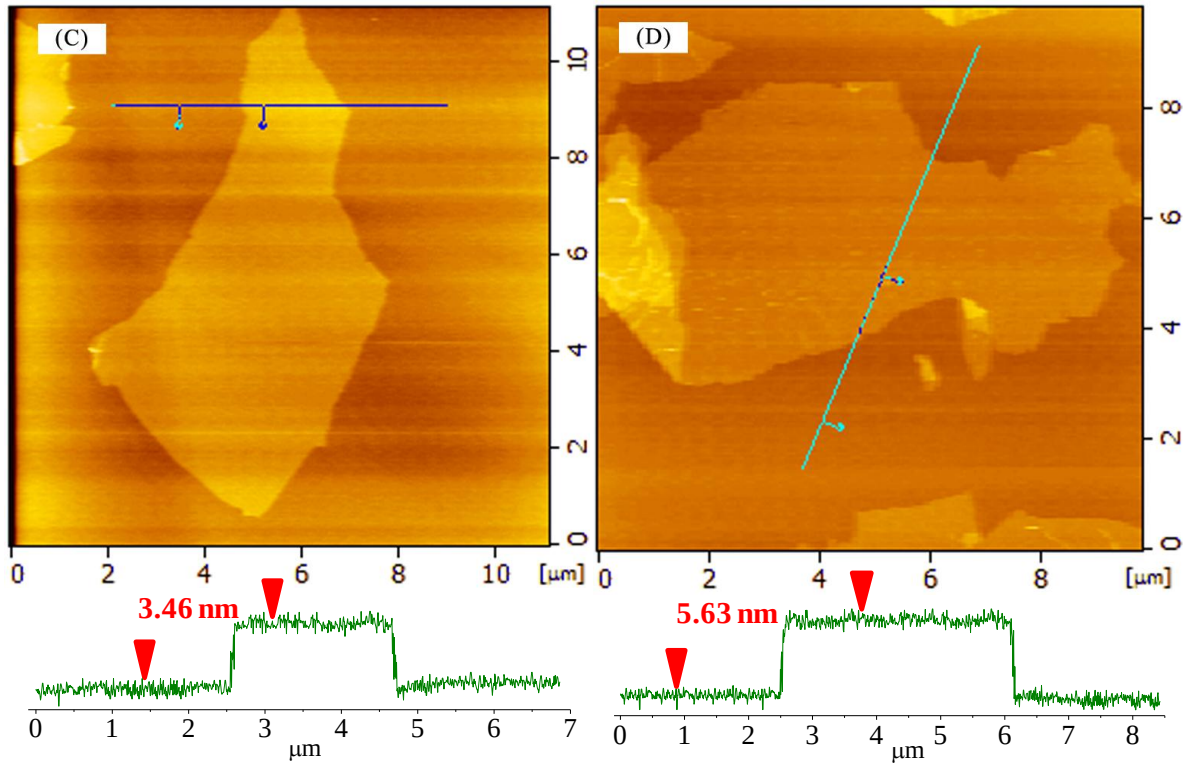

Fig. 4 AFM analyses of (A) GO, (B) H-RGO, (C) PDA-RGO and (D) PF-PDA-RGO nanosheets.

AFM were further used to investigate the 2-D surface morphology and the thickness of the GO and surface functionalized RGO. As shown in Fig. 4A, the individual GO sheet shows some wrinkles and has a thickness of about 0.87 nm, which is thicker than that of ideal graphene because of the existence of oxygen-containing groups.[62] However, the H-RGO nanosheets exhibit an easy-folding state and have a thickness of about 1.24 nm (Fig. 4B), indicating that the H-RGO nanosheets are prone to aggregate because of the removal of oxygen-containing groups and exhibit a poor dispersion in the solution. Fig. 4C and D show the typical AFM analyses of PDA-RGO and PF-PDA-RGO, respectively. Both of the nanosheets exhibit a flat surface profile and the thickness increase to 3.46 nm for PDA-RGO and 5.63 nm for PF-PDA-RGO, indicating that the PDA layer and PF polymer have been uniformly and successfully coated onto the surface of RGO.

Preparation and characterization of P(VDF-HFP)/RGO nanocomposite films

P(VDF-HFP) nanocomposite films containing different volume contents of RGO (*i.e.*, H-RGO, PDA-RGO and PF-PDA-RGO) were prepared by solution blending and hot compression molding.

The freeze-fractured cross sections of the nanocomposite films with 0.5 vol% of RGO were characterized by SEM to investigate the microstructure of the nanocomposites. One can see from Fig. 5 that the microstructure of the P(VDF-HFP) nanocomposites is closely associated with funcationalization of the RGO. In the case of P(VDF-HFP)/H-RGO, the fractured surface is rough and filler-matrix detachment can be observed, indicating weak interaction between H-RGO and matrix (Fig. 5B). Additionally, there are many defects and voids in the nanocomposite film, suggesting the poor compatibility and dispersion of H-RGO in P(VDF-HFP). In contrast, the relatively smooth fractured surface of P(VDF-HFP)/PDA-RGO shown in Fig. 5C suggests the stronger interfacial adhesion between PDA-RGO and matrix. The improved compatibility between PDA-RGO and P(VDF-HFP) matrix should be attributed to the formation of hydrogen bonds between the PDA and matrix.[14] It has been proved in previous reports that the hydroxyl and amine groups on the surface of fillers can provide hydrogen bonds with fluorine atoms of fluoro-polymer matrix, which can improve the interfacial adhesion and compatibility between filler and matrix. In P(VDF-HFP)/PF-PDA-RGO, the fractured surface of the nanocomposite film become smoother and no visible voids can be found (Fig. 5D). There is also no evidence of filler-matrix detachment. This result indicate that the grafting of fluoro-polymer chains can further provide strong interchain forces with the P(VDF-HFP) matrix and improve the interfacial adhesion between PF-PDA-RGO and matrix.[20] The excellent microstructural integrity combined with a small loading of RGO fillers make the P(VDF-HFP) nanocomposites have excellent flexibility. As shown in Fig. 5E and F, the P(VDF-HFP)/PF-PDA-RGO nanocomposite film is capable of being rolled, which is highly desirable for flexible dielectric materials.

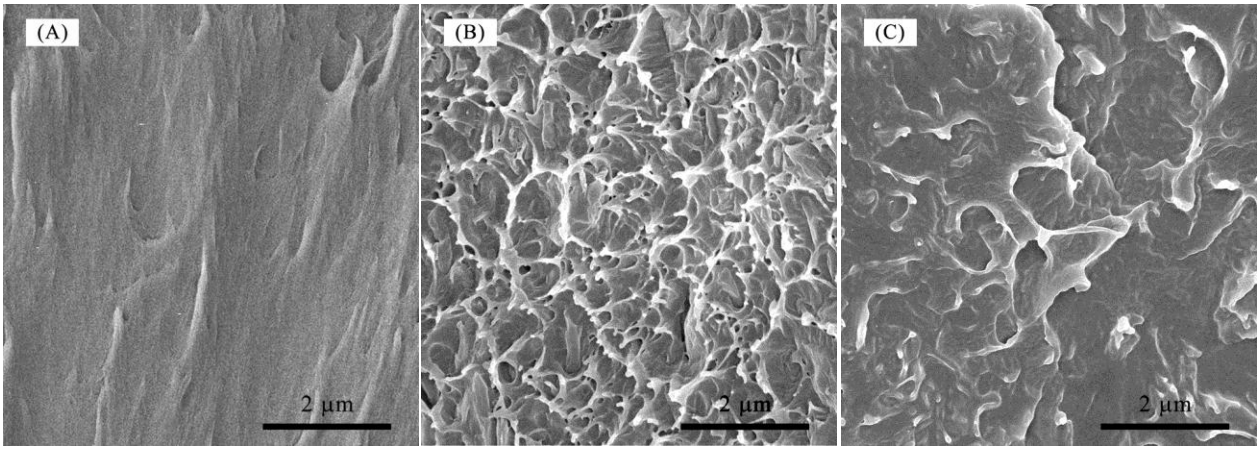

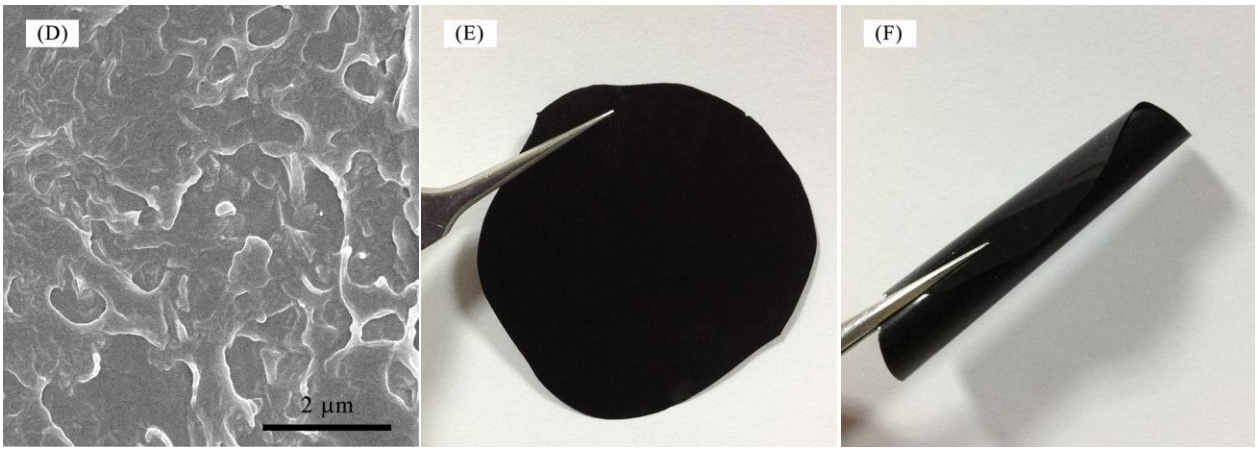

Fig. 5 SEM images of the freeze-fractured cross sections of (A) pure P(VDF-HFP) film and P(VDF-HFP)/RGO nanocomposite films with 0.5 vol% of RGO nanosheets: (B) H-RGO, (C) PDA-RGO, and (D) PF-PDA-RGO; Digital photos of the flexible P(VDF-HFP)/PF-PDA-RGO nanocomposite film with 2 vol% of RGO nanosheets: (E) before rolling, and (F) after rolling.

It has been confirmed in previous researches that the interface between nanofiller and polymer matrix is crucial to the thermal, electrical, mechanical, and other properties of the polymer nanocomposites.[63-66] Here, the role of RGO/P(VDF-HFP) interface in determining the thermal properties of the nanocomposites were investigated. First, the thermal stability of pure P(VDF-HFP) and the P(VDF-HFP)/RGO nanocomposites were evaluated by TGA in nitrogen atmosphere. As shown in Fig. 6A, unlike the TGA curve of the pure P(VDF-HFP), all the P(VDF-HFP)/RGO nanocomposites exhibit two stages of weight loss. The first stage with a slight weight loss appears from 300 to about 450 ℃, which is ascribed to the degradation of the surface modifiers and carbon backbones of the RGO. The second stage with a major weight loss takes place from about 450 to 1000 ℃, which is assigned to the degradation of the P(VDF-HFP) matrix. The degradation profiles of the nanocomposites are similar, indicating that the introduction of RGO nanosheets did not significantly alter the degradation mechanism of the P(VDF-HFP) matrix. However, compared with the pure P(VDF-HFP), the degradation of the nanocomposites show a remarkable hysteresis. One can see that the curves of all the nanocomposites shift to high temperatures in comparison with the pure P(VDF-HFP). For example, at the weight loss of 10%, the corresponding temperature ($T_{10\%}$) for pure P(VDF-HFP) is 445.4 ℃, which is increased to 462.7, 475.2, and 488.6 ℃ for the nanocomposites with 1.0 vol% of H-RGO, PDA-RGO, and PF-PDA-RGO, respectively. This phenomenon has been reported in numerous previous works, which can be understood by the following explanations: i) the introduction of RGO nanosheets

restricts the thermal motion of the polymer chains, effectively promoting the thermal stability of the polymer matrix; ii) the differences of interfacial adhesion between the RGO and matrix lead to different thermal stability of their nanocomposites.[39, 64] It should also be noted that when the temperature reaches up to 1000 ℃, there still exist a small amount of carbon residues for all samples because of the inherent flame-retardancy of the P(VDF-HFP) matrix. However, after introducing the RGO nanosheets, the values of carbon residues of the nanocomposites are lower than that of pure P(VDF-HFP). The most likely reason for such an abnormal phenomenon is the formation of 3-D networks by the carbon backbones of RGO nanosheets, which inhibits the formation of compact char and promotes the further degradation of the carbon residues at high temperature. Generally, the well dispersed RGO nanosheets tend to form excellent 3-D networks in polymer matrix. Thus, the fact that the P(VDF-HFP)/PF-PDA-RGO shows the lowest weight fraction of carbon residue may suggest the best dispersion of PF-PDA-RGO in P(VDF-HFP) matrix.

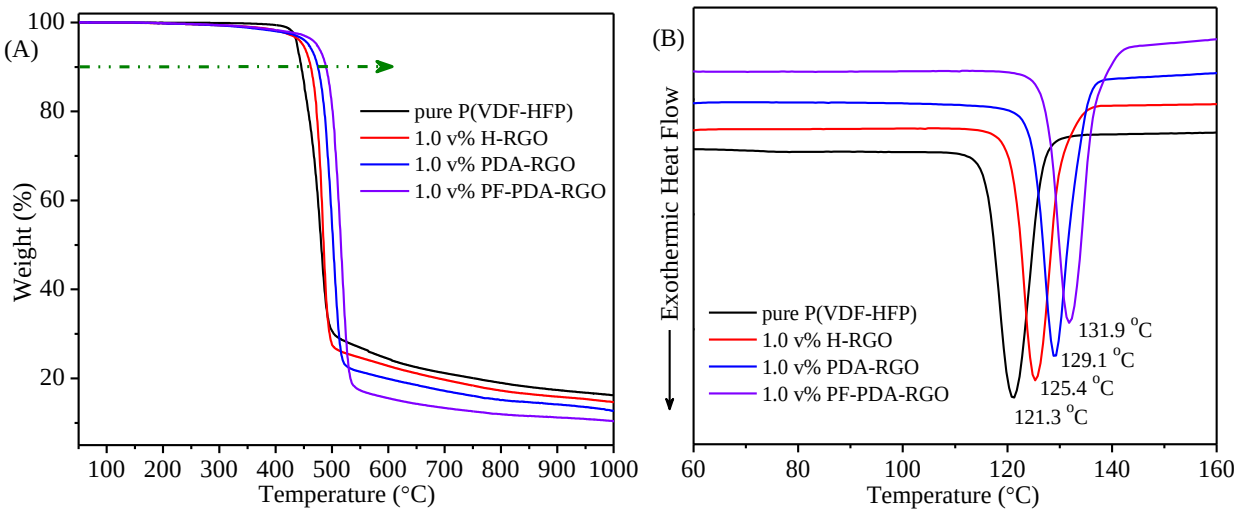

Fig. 6 (A) TGA curves and (B) DSC cooling curves of pure P(VDF-HFP) and P(VDF-HFP)/RGO nanocomposites with 1.0 vol% of RGO nanosheets.

The crystallization process of the pure P(VDF-HFP) and P(VDF-HFP)/RGO were also investigated by DSC. As shown in Fig. 6B, the crystallization temperatures (T_c) of the nanocomposites obviously shift to high temperatures after the introduction of the RGO nanosheets. For example, the T_c of the pure P(VDF-HFP) is 121.3 ℃, whereas the T_c values are increased to 125.4, 129.1, and 131.9 ℃ for the nanocomposites with 1.0 vol% of H-RGO,

PDA-RGO, and PF-PDA-RGO, respectively. It has been proved in previous works that the well-dispersed nanofillers in polymer matrix can act as nucleation sites and inhibit the movement of polymer chain segment, which can improve the T_c of polymer nanocomposites.[67] Therefore, the increment of T_c values for P(VDF-HFP)/RGO nanocomposites is because of the presence of RGO nanosheets. The highest T_c value for P(VDF-HFP)/PF-PDA-RGO nanocomposites further confirm that the best dispersion of PF-PDA-RGO and the strongest interfacial adhesion between PF-PDA-RGO and polymer matrix.

Dielectric properties of P(VDF-HFP)/RGO nanocomposite films

The dielectric properties of the P(VDF-HFP)/RGO nanocomposite films were investigated by a broadband dielectric spectroscopy at room temperature. Fig. 7 shows the variations of dielectric constant and dielectric loss tangent (tan δ) of P(VDF-HFP)/H-RGO, P(VDF-HFP)/PDA-RGO, and P(VDF-HFP)/PF-PDA-RGO nanocomposite films as a function of frequency with different volume fractions of RGO. The similar feature of the samples is that both of the dielectric constant and tan δ are increased with the increase of RGO contents. When the volume fraction of RGO is lower than about 1.0 vol%, the dielectric constant and tan δ of the nanocomposite films are increased gradually with the increase of RGO contents and show a weak dependence on the frequency. Starting from 1.0 vol% of RGO, the dielectric constant and tan δ of the nanocomposites not only exhibit dramatic increase with the further increase of RGO and but also show strong dependence on the frequency. This phenomenon is widely observed in previous studies, which is the typical feature of the percolative nanocompsite systems filled by graphene nanosheets or other conductive fillers.[21-23, 33, 34, 39, 40]

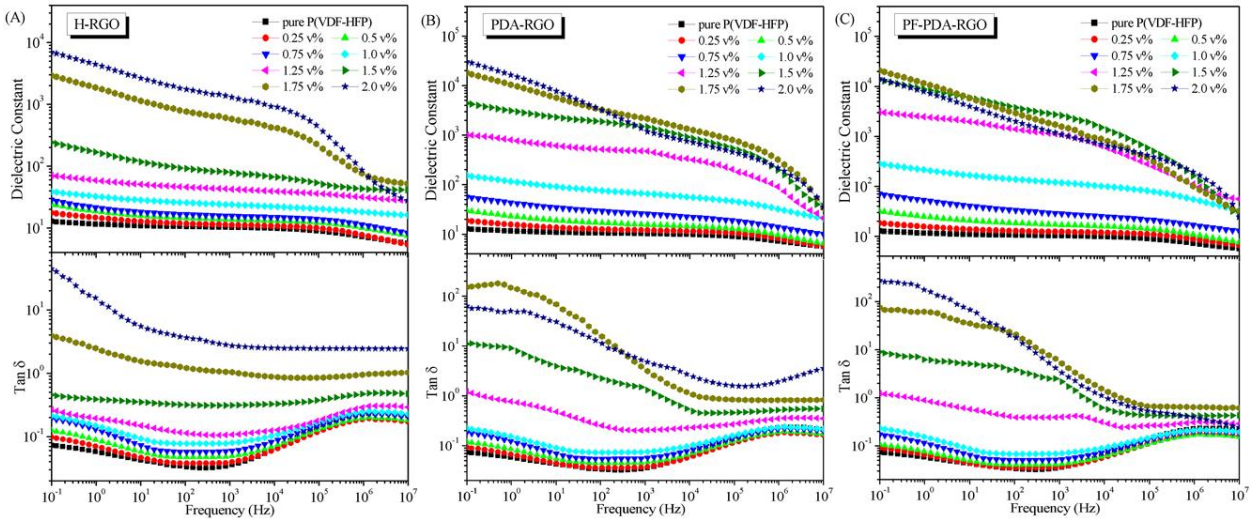

Fig. 7 Frequency dependence of dielectric constant and dielectric loss tangent (tan δ) of pure P(VDF-HFP) and P(VDF-HFP)/RGO nanocomposites with (A) H-RGO, (B) PDA-RGO, and (C) PF-PDA-RGO.

For the composites filled with conductive RGO nanosheets, when the filler content approaches the percolation threshold, the values of dielectric constant can be predicted by the following percolation theory power law,[45]

$$\varepsilon = \varepsilon_m (f_c - f_{RGO})^{-s}, \text{ for } \quad f_{RGO} < f_c \qquad (1)$$

where ε is the dielectric constant of the composites, ε_m is the dielectric constant of the polymer matrix, f_{RGO} is the volume fraction of RGO in composites, f_c is the critical volume fraction of the RGO at the percolation threshold, and s is the critical exponent related to the material properties. According to equation 1, huge dielectric constant will be obtained when the f_{RGO} infinitesimally close to the f_c. Therefore, the combination of ε and f_c is also useful to evaluate the effective loading content of RGO nanosheets. A high dielectric constant ε and a low percolation threshold f_c indicate a high enhancing effect on the dielectric properties of the nanocompsites.

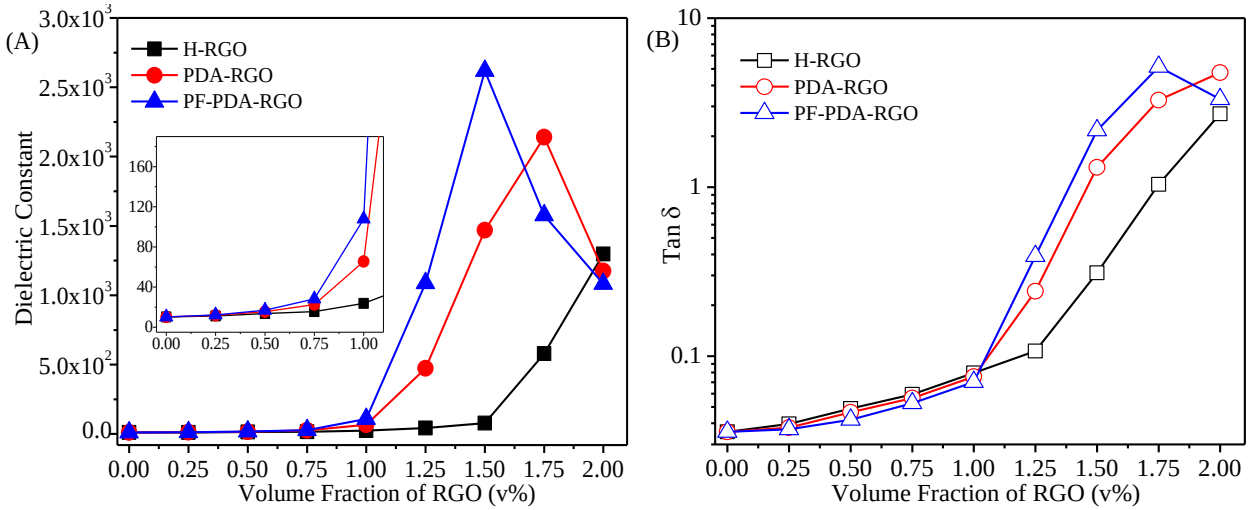

Fig. 8 (A) Dielectric constant and (B) dielectric loss tangent (tan δ) of P(VDF-HFP)/RGO nanocomposites with different volume fraction of RGO nanosheets at 1 kHz. Inset in (A) is the corresponding dielectric constants of nanocomposites with lower content of RGO.

It should be noted in Fig. 7 that at a given frequency and at the same f_{RGO}, the magnitude of the dielectric parameters of the nanocomposites are associated with surface functionalization of RGO. To gain more clear insights, we extracted the dielectric constant and tan δ of different nanocomposite films with various volume fractions of RGO nanosheets at 1 kHz. One can see from Fig. 8A that, when the content of RGO is lower than about 1.0 vol%, the dielectric constants of all samples are nearly equal and increase slightly with the increase of RGO contents. However, when the volume fraction of RGO is higher than about 1.0 %, the dielectric constants of all samples exhibit significant difference and increase rapidly with the increase of RGO contents, especially for the nanocomposites filled with PDA-RGO and PF-PDA-RGO nanosheets. The significant difference of dielectric constants at relatively high RGO contents should be mainly originated from the various RGO dispersion state. The best linear fits for the experimental dielectric constants of the nanocomposites were carried out and the results are shown in Fig S4 (*see* ESI) according to equation 1. The fits give f_c values of P(VDF-HFP)/H-RGO, P(VDF-HFP)/PDA-RGO, and P(VDF-HFP)/PF-PDA-RGO nanocomposites 1.52 vol%, 1.19 vol%, and 1.06 vol%, respectively. It can be found that the P(VDF-HFP)/PF-PDA-RGO nanocomposites has the lowest f_c value, which further indicates the best dispersion and compatibility of PF-PDA-RGO in P(VDF-HFP) matrix. Generally, in order to realize high dielectric constant and maintain the flexibility of the dielectric materials, the relatively low

loading of fillers is very important for a percolative nanocompsite system, which is highly depended on the value of f_c. Therefore, the lowest f_c value of P(VDF-HFP)/PF-PDA-RGO nanocomposite films is very promising for practical application. In order to investigate the error range of dielectric properties, three different capacitors for each sample were measured to evaluate the dielectric constant distribution. The results reveal that all the samples exhibit narrow distribution of dielectric constant and show a small error range (Table S1 in ESI).

The dielectric loss tan δ of the nanocomposites show the similar dependence on the RGO content in comparison with the dielectric constant, as shown in Fig. 8B. The tan δ of all nanocomposite samples are maintained in a relatively low level (< 0.1) when the $f_{RGO} < f_c$, whereas an abrupt increase of tan δ can be observed near the percolation threshold. In addition, tan δ increases fast after the percolation threshold. These are the typical features of percolative systems.[22, 23, 33, 45] Generally, the dielectric loss of dielectric materials mainly originates from the conduction process, interfacial polarization and molecular dipole movement.[68] In the case of percolative systems with the filler content lower than f_c, the dielectric loss is mainly originates from the interfacial polarization.[25] As the filler content increases beyond the f_c, the conductive networks are formed and thus the conduction loss becomes dominant and the dielectric loss exhibit a dramatic increase.[21, 40] It should be noted from Fig. 8B that when the RGO contents is lower than about 1.0 vol%, the P(VDF-HFP)/PF-PDA-RGO nanocomposite films show the lowest dielectric loss. When the RGO contents is higher than about 1.0 vol%, however, the P(VDF-HFP)/PF-PDA-RGO start to show the highest dielectric loss among the three types of nanocomposites. These results can be understood by the follow explanations: i) when $f_{RGO} <$ 1.0 vol%, the interfacial polarization is dominant in determining the dielectric loss. The strong interfacial adhesion between the PF-PDA-RGO nanosheets and P(VDF-HFP) matrix results in weak interfacial polarization and thus low dielectric loss for the nanocomposites; ii) when $f_{RGO} >$ 1.0 vol%, the conduction process becomes dominant in determining the dielectric loss. The PF-PDA-RGO nanosheets are well dispersed in P(VDF-HFP), which causes more compact conductive networks and thus higher dielectric loss.

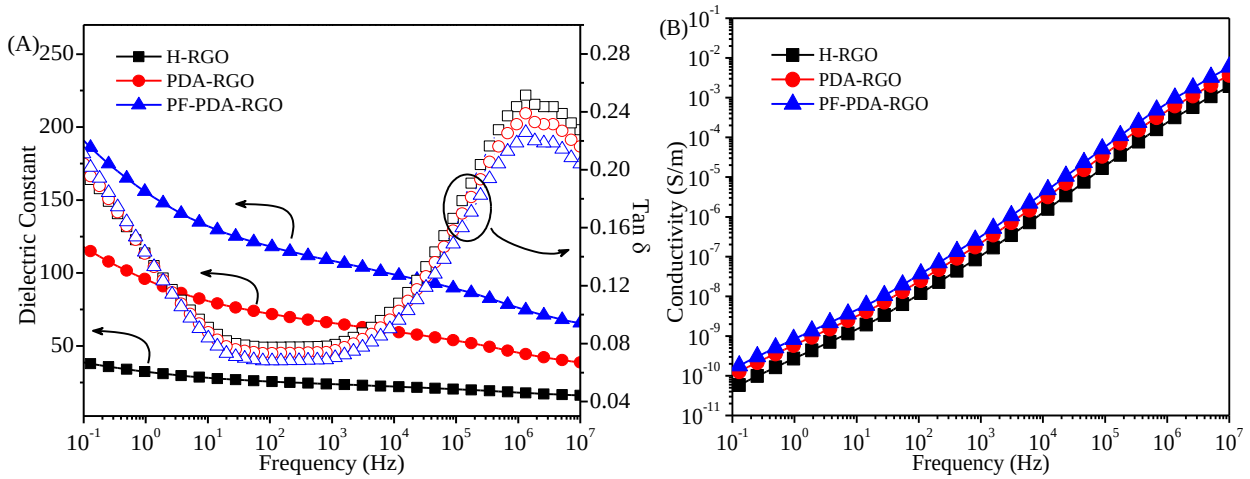

Fig. 9 (A) Dielectric constant and dielectric loss tangent (tan δ) and (B) conductivity of P(VDF-HFP)/RGO nanocomposites with 1.0 vol% of RGO nanosheets as a function of frequency.

To further investigate the dielectric properties of the nanocomposites, we compared the frequency dependent dielectric constant and dielectric loss tangent of the nanocomposites with 1.0 vol% RGO. The nanocomposites with 1.0 vol% RGO are chosen because that this concentration is slightly lower than the percolation threshold of the nanocomposites. In such a case, the nanocomposites not only have a high dielectric constant but also exhibit a low dielectric loss. As shown in Fig. 9A, the dielectric constant of nanocomposites with PF-PDA-RGO is obviously higher than that of the others over the whole frequency range. For example, the dielectric constant is 107.9 for P(VDF-HFP)/PF-PDA-RGO at 1 kHz, whereas the corresponding values are 23.8 and 65.5 for P(VDF-HFP)/H-RGO and P(VDF-HFP)/PDA-RGO, respectively. The increment of the dielectric constant in our nanocomposites can be explained by the microcapacitor model.[45] The PF-PDA-RGO nanosheets show the better dispersion in the P(VDF-HFP) matrix in comparison with other RGO nanosheets, which should give rise to the formation of more microcapacitors and thus higher dielectric constant. Fig. 9A also presents the frequency dependence of dielectric loss tan δ of the samples. It should be noted that in the low frequency range of 0.1~10 Hz, tan δ of P(VDF-HFP)/PF-PDA-RGO nanocomposites is slightly higher than that of the others. This is reasonable because the excellent dispersion of PF-PDA-RGO nanosheets can increase the interfacial area between the fillers and matrix, which leads to stronger interfacial polarization in the low frequency range. However, when the frequency is greater than 10 Hz, tan δ of the nanocomposites show an order of

P(VDF-HFP)/PF-PDA-RGO < P(VDF-HFP)/PDA-RGO < P(VDF-HFP)/H-RGO and their corresponding tan δ values are 0.070, 0.075 and 0.079 at 1 kHz, respectively. As mentioned earlier, the H-RGO nanosheets show poor dispersion and compatibility in P(VDF-HFP) and there are many defects and voids in the nanocomposites (*see* Fig. 5B). Compared with H-RGO, the dispersion of PDA-RGO get greatly enhanced and the compatibility between PDA-RGO and P(VDF-HFP) is also improved by the formation of hydrogen bonds. In this case, the migration and accumulation of space charge within the P(VDF-HFP)/PDA-RGO nanocompasites can be significantly suppressed and the movement of the molecular dipoles can be restricted in the high frequencies, which leads to relatively lower dielectric loss in comparison with P(VDF-HFP)/H-RGO nanocompasites.[69] Furthermore, the fluoro-polymer chains grafted on the PDA-RGO surfaces can further improve the dispersion and compatibility of PF-PDA-RGO in matrix. In addition, the surface grafted fluoro-polymer chains can be entangled with the chains of P(VDF-HFP) matrix and thus further enhancing the interfacial adhesion of P(VDF-HFP)/PF-PDA-RGO nanocomposites, resulting in further limitation on the movement of molecular dipoles and thus suppressed dielectric loss.[20]

In order to investigate the dielectric constant stability of our materials, the dielectric properties of samples with three folding states were measured (as illustrated in Figure S5). The dielectric constants of our samples with different folding states were provided in Table S2 (*see* ESI), the results reveal that all the samples exhibit stable dielectric performance and show a small error range under different folding states.

For practical applications, the insulating behavior is also a great important property for dielectric materials. Fig. 9B shows the alternating current (ac) conductivities of the nanocomposites with 1.0 vol% RGO. It can be found that the conductivities of all samples show strong frequency dependence over the whole measurement frequency range. Despite having slightly higher values, the conductivities of the P(VDF-HFP)/PF-PDA-RGO nanocomposites still maintain in a relatively low level (*e.g.*, about 1.48×10^{-10} S/m at 0.1 Hz), indicating an excellent insulating behavior when the RGO content is 1.0 vol%. This result, in combination with the excellent dielectric properties mentioned earlier, indicate that the fluoro-polymer functionalized RGO is a promising candidate for preparing high performance flexible nanodielectric materials.

Taking the aforementioned high thermal stability, high dielectric constant and low dielectric

loss at power frequency (*e.g.*, 50 Hz), excellent dielectric constant stability and mechanical flexibility, the P(VDF-HFP)/PF-PDA-RGO nanocomposites are more attractive for stress control application in power cable terminations[70, 71]. In power cable terminations, high dielectric constant materials are required to release the highly concentrated electric stress at the insulation cutback point to avoid the surface discharge and air breakdown which can cause cable failure. The high dielectric constant and dielectric constant stability are important to reduce the electric stress, while the high thermal stability and low dielectric loss and excellent mechanical flexibility are also important to increase the lifetime and improve the reliability of the cable terminations.

Conclusions

In this work, fluoro-polymer functionalized RGO were successfully prepared by the self-polymerization of dopamine and the subsequent Michael addition of thiol-terminated poly(trifluoroethyl acrylate). The P(VDF-HFP) based nanocomposites filled with H-RGO, PDA-RGO and PF-PDA-RGO were prepared, and their dielectric properties were investigated. Our results showed that, both of the PDA coating and the grafting of PF polymer chains can effectively enhance the dispersion and compatibility of the RGO nanosheets in P(VDF-HFP) matrix. Additionally, the surface-grafted fluoro-polymer chains can be entangled with the polymer chains of matrix, which can further strengthen the interfacial adhesion between RGO and fluoro-polymer matrix. Dielectric measurements revealed that the percolation threshold of PF-PDA-RGO/P(VDF-HFP) is 1.06 vol%, which was obviously lower than that the PDA-RGO/P(VDF-HFP) and H-RGO/P(VDF-HFP). When the RGO fraction is lower and near the percolation threshold, the P(VDF-HFP)/PF-PDA-RGO nanocomposites exhibit the highest dielectric constant over the whole frequency range, and show the lowest dielectric loss in the high frequencies (*i.e.*, 10 ~ 10^7 Hz). More importantly, the P(VDF-HFP)/PF-PDA-RGO nanocomposites still exhibit an excellent insulating behavior when $f_{RGO} < f_c$. All these results suggest that the fluoro-polymer functionalized RGO is a promising candidate for preparing high performance flexible nanodielectric materials used in electronic and electric industry.

Acknowledgement

The authors gratefully acknowledge supports from the National Natural Science Foundation of China (Nos. 51107081, 51277117) and the Special Fund of the National Priority Basic Research of China under Grant 2014CB239503. X.Y.H. thanks the 2013 SMC Excellent Young Faculty Award of Shanghai Jiao Tong University for finical support. This work was sponsored by Shanghai Pujiang Program under Grant PJ14D018 (X.Y.H.) and the State Key Laboratory of Power System under Grant SKLD13KZ02 in Tsinghua University in part.

Notes

Electronic Supplementary Information (ESI) available: See DOI: 10.1039/b000000x/

References

1. Z. M. Dang, J. K. Yuan, S. H. Yao and R. J. Liao, *Adv. Mater.*, 2013, **25**, 6334-6365.
2. R. P. Ortiz, A. Facchetti and T. J. Marks, *Chem. Rev.*, 2010, **110**, 205-239.
3. Y. Wang, X. Zhou, Q. Chen, B. J. Chu and Q. M. Zhang, *IEEE Trans. Dielectr. Electr. Insul.*, 2010, **17**, 1036-1042.
4. Z. M. Dang, J. K. Yuan, J. W. Zha, T. Zhou, S. T. Li and G. H. Hu, *Prog. Mater. Sci.*, 2012, **57**, 660-723.
5. Q. Wang and L. Zhu, *J. Polym. Sci., Part B: Polym. Phys.*, 2011, **49**, 1421-1429.
6. K. Yang, X. Y. Huang, M. Zhu, L. Y. Xie, T. Tanaka and P. K. Jiang, *ACS Appl. Mater. Interfaces*, 2014, **6**, 1812-1822.
7. X. Zhang, W. W. Chen, J. J. Wang, Y. Shen, L. Gu, Y. H. Lin and C. W. Nan, *Nanoscale*, 2014, **6**, 6701-6709.
8. K. Yang, X. Y. Huang, L. Y. Xie, C. Wu, P. K. Jiang and T. Tanaka, *Macromol. Rapid Commun.*, 2012, **33**, 1921-1926.
9. H. X. Tang and H. A. Sodano, *Nano Lett.*, 2013, **13**, 1373-1379.
10. H. X. Tang, Y. R. Lin and H. A. Sodano, *Adv. Energy Mater.*, 2013, **3**, 451-456.
11. L. Y. Xie, X. Y. Huang, C. Wu and P. K. Jiang, *J. Mater. Chem.*, 2011, **21**, 5897-5906.
12. K. H. Lee, J. Kao, S. S. Parizi, G. Caruntu and T. Xu, *Nanoscale*, 2014, **6**, 3526-3531.
13. M. F. Lin and P. S. Lee, *J. Mater. Chem. A*, 2013, **1**, 14455-14459.
14 Y. Song, Y. Shen, H. Y. Liu, Y. H. Lin, M. Li and C. W. Nan, *J. Mater. Chem.*, 2012, **22**, 8063-8068.
15 N. Guo, S. A. DiBenedetto, P. Tewari, M. T. Lanagan, M. A. Ratner and T. J. Marks, *Chem. Mater.*, 2010, **22**, 1567-1578.
16 P. Kim, N. M. Doss, J. P. Tillotson, P. J. Hotchkiss, M.-J. Pan, S. R. Marder, J. Li, J. P. Calame and J. W. Perry, *ACS Nano*, 2009, **3**, 2581-2592.
17 J. Li, P. Khanchaitit, K. Han and Q. Wang, *Chem. Mater.*, 2010, **22**, 5350-5357.
18 L. Y. Xie, X. Y. Huang, Y. H. Huang, K. Yang and P. K. Jiang, *ACS Appl. Mater. Interfaces*, 2013, **5**, 1747-1756.
19 L. Y. Xie, X. Y. Huang, B.-W. Li, C. Y. Zhi, T. Tanaka and P. K. Jiang, *Phys. Chem. Chem. Phys.*, 2013, **15**, 17560-17569.
20 K. Yang, X. Y. Huang, Y. H. Huang, L. Y. Xie and P. K. Jiang, *Chem. Mater.*, 2013, **25**, 2327-2338.
21 L. Wang and Z. M. Dang, *Appl. Phys. Lett.*, 2005, **87**, 042903.
22 H. Y. Liu, Y. Shen, Y. Song, C. W. Nan, Y. H. Lin and X. P. Yang, *Adv. Mater.*, 2011, **23**, 5104-5108.
23 Y. Shen, Y. H. Lin, M. Li and C. W. Nan, *Adv. Mater.*, 2007, **19**, 1418-1422.
24 Y. Xunqian, J. F. Capsal and D. Guyomar, *Appl. Phys. Lett.*, 2014, **104**, 052913.
25 C. W. Nan, Y. Shen and J. Ma, *Annu. Rev. Mater. Res.*, 2010, **40**, 131-151.
26 A. K. Geim, *Science*, 2009, **324**, 1530-1534.

27 A. Y. W. Sham and S. M. Notley, *Soft Matter*, 2013, **9**, 6645-6653.
28 H. Kim, A. A. Abdala and C. W. Macosko, *Macromolecules*, 2010, **43**, 6515-6530.
29 L. P. Yang, J. H. Kong, W. A. Yee, W. S. Liu, S. L. Phua, C. L. Toh, S. Huang and X. H. Lu, *Nanoscale*, 2012, **4**, 4968-4971.
30 C. Wu, X. Y. Huang, G. L. Wang, L. B. Lv, G. Chen, G. Y. Li and P. K. Jiang, *Adv. Funct. Mater.*, 2013, **23**, 506-513.
31 M. Yoonessi and J. R. Gaier, *ACS Nano*, 2010, **4**, 7211-7220.
32 L. L. Jiang and Z. J. Fan, *Nanoscale*, 2014, **6**, 1922-1945.
33 C. Wu, X. Y. Huang, G. L. Wang, X. F. Wu, K. Yang, S. T. Li and P. K. Jiang, *J. Mater. Chem.*, 2012, **22**, 7010-7019.
34 J.-Y. Kim, W. H. Lee, J. W. Suk, J. R. Potts, H. Chou, I. N. Kholmanov, R. D. Piner, J. Lee, D. Akinwande and R. S. Ruoff, *Adv. Mater.*, 2013, **25**, 2308-2313.
35 Z. Wang, J. K. Nelson, H. Hillborg, S. Zhao and L. S. Schadler, *Adv. Mater.*, 2012, **24**, 3134-3137.
36 C. Min, D. M. Yu, J. Y. Cao, G. L. Wang and L. H. Feng, *Carbon*, 2013, **55**, 116-125.
37 W. S. Tong, Y. H. Zhang, L. Yu, X. L. Luan, Q. An, Q. Zhang, F. Z. Lv, P. K. Chu, B. Shen and Z. L. Zhang, *J. Phys. Chem. C*, 2014, **118**, 10567-10573.
38 F. Wen, Z. Xu, S. B. Tan, W. M. Xia, X. Y. Wei and Z. C. Zhang, *ACS Appl. Mater. Interfaces*, 2013, **5**, 9411-9420.
39 J. H. Yu, X. Y. Huang, C. Wu and P. K. Jiang, *IEEE Trans. Dielectr. Electr. Insul.*, 2011, **18**, 478-484.
40 H. Tang, G. J. Ehlert, Y. Lin and H. A. Sodano, *Nano Lett.*, 2012, **12**, 84-90.
41 Y. S. Ye, Y. N. Chen, J. S. Wang, J. Rick, Y. J. Huang, F. C. Chang and B. J. Hwang, *Chem. Mater.*, 2012, **24**, 2987-2997.
42 H. J. Salavagione, G. Martinez and G. Ellis, *Macromol. Rapid Commun.*, 2011, **32**, 1771-1789.
43 T. Ramanathan, A. A. Abdala, S. Stankovich, D. A. Dikin, M. Herrera-Alonso, R. D. Piner, D. H. Adamson, H. C. Schniepp, X. Chen, R. S. Ruoff, S. T. Nguyen, I. A. Aksay, R. K. Prud'homme and L. C. Brinson, *Nat. Nanotechnol.*, 2008, **3**, 327-331.
44 T. Kuila, A. K. Mishra, P. Khanra, N. H. Kim and J. H. Lee, *Nanoscale*, 2013, **5**, 52-71.
45 D. Wang, Y. Bao, J.-W. Zha, J. Zhao, Z.-M. Dang and G.-H. Hu, *ACS Appl. Mater. Interfaces*, 2012, **4**, 6273-6279.
46 H. Lee, Y. Lee, A. R. Statz, J. Rho, T. G. Park and P. B. Messersmith, *Adv. Mater.*, 2008, **20**, 1619-1623.
47 H. Lee, S. M. Dellatore, W. M. Miller and P. B. Messersmith, *Science*, 2007, **318**, 426-430.
48 L. Zhang, J. J. Wu, Y. X. Wang, Y. H. Long, N. Zhao and J. Xu, *J. Am. Chem. Soc.*, 2012, **134**, 9879-9881.
49 L. Q. Xu, W. J. Yang, K.-G. Neoh, E.-T. Kang and G. D. Fu, *Macromolecules*, 2010, **43**, 8336-8339.
50 J. Yan, L. P. Yang, M.-F. Lin., J. Ma., X. H. Lu. and P. S. Lee, *Small*, 2013, **9**, 596-603.
51 C. Cheng, S. Nie, S. Li, H. Peng, H. Yang, L. Ma, S. Sun and C. Zhao, *J. Mater. Chem. B*, 2013, **1**, 265-275.
52 S. M. Kang, S. Park, D. Kim, S. Y. Park, R. S. Ruoff and H. Lee, *Adv. Funct. Mater.*, 2011, **21**, 108-112.
53 L. Yang, W. A. Yee, S. L. Phua, J. Kong, H. Ding, J. W. Cheah and X. Lu, *RSC Adv.*, 2012, **2**, 2208-2210.
54 Y. Liu, K. Ai and L. Lu, *Chem. Rev.*, 2014, **114**, 5057-5115.
55 Z. Zhang, J. Zhang, B. Zhang and J. Tang, *Nanoscale*, 2013, **5**, 118-123.
56 C. Wu, X. Y. Huang, X. F. Wu, L. Y. Xie, K. Yang and P. K. Jiang, *Nanoscale*, 2013, **5**, 3847-3855.
57 Y. Xu, H. Bai, G. Lu, C. Li and G. Q. Shi, *J. Am. Chem. Soc.*, 2008, **130**, 5856-5857.
58 W. Q. Shen, Q. A. Qiu, Y. Wang, M. A. Miao, B. S. Li, T. S. Zhang, A. N. Cao and Z. S. An, *Macromol. Rapid Commun.*, 2010, **31**, 1444-1448.
59 D. A. Dikin, S. Stankovich, E. J. Zimney, R. D. Piner, G. H. B. Dommett, G. Evmenenko, S. T. Nguyen and R. S. Ruoff, *Nature*, 2007, **448**, 457-460.
60 E. Leivo, T. Wilenius, T. Kinos, P. Vuoristo and T. Mäntylä, *Prog. Org. Coat.*, 2004, **49**, 69-73.
61 S. Guo, D. Wen, Y. Zhai, S. Dong and E. Wang, *ACS Nano*, 2010, **4**, 3959-3968.
62 D. R. Dreyer, S. Park, C. W. Bielawski and R. S. Ruoff, *Chem. Soc. Rev.*, 2010, **39**, 228-240.

63 D. L. Ma, T. A. Hugener, R. W. Siegel, A. Christerson, E. Martensson, C. Onneby and L. S. Schadler, *Nanotechnology*, 2005, **16**, 724-731.

64 A. Bansal, H. Yang, C. Li, B. C. Benicewicz, S. K. Kumar and L. S. Schadler, *J. Poly. Sci. Part B: Poly. Phys.*, 2006, **44**, 2944-2950.

65 L. S. Schadler, S. K. Kumar, B. C. Benicewicz, S. L. Lewis and S. E. Harton, *MRS Bull.*, 2007, **32**, 335-340.

66 B. Natarajan, T. Neely, A. Rungta, B. C. Benicewicz and L. S. Schadler, *Macromolecules*, 2013, **46**, 4909-4918.

67 L. S. Schadler, *Nat Mater*, 2007, **6**, 257-258.

68 X. Y. Huang, C. Y. Zhi, P. K. Jiang, D. Golberg, Y. Bando and T. Tanaka, *Nanotechnology*, 2012, **23**, 455705.

69 M. Roy, J. K. Nelson, R. K. MacCrone, L. S. Schadler, C. W. Reed and R. Keefe, *IEEE Trans. Dielectr. Electr. Insul.*, 2005, **12**, 629-643.

70 X. Y. Huang, L. Y. Xie, K. Yang, C. Wu, P. K. Jiang, S. T. Li, S. Wu, K. Tatsumi and T. Tanaka, *IEEE Trans. Dielectr. Electr. Insul.*, 2014, **21**, 467-479.

71 X. Y. Huang and P. K. Jiang, *Adv. Mater.*, 2014, DOI: 10.1002/adma.201401310

TOC Graphic

Fluoro-polymer Functionalized Graphene for Flexible Ferroelectric Polymer-based High-*k* Nanocomposites with Suppressed Dielectric Loss and Low Percolation Threshold

Ke Yang[†], Xingyi Huang*[,†], Lijun Fang[†], Jinliang He[‡], and Pingkai Jiang*[†,§]

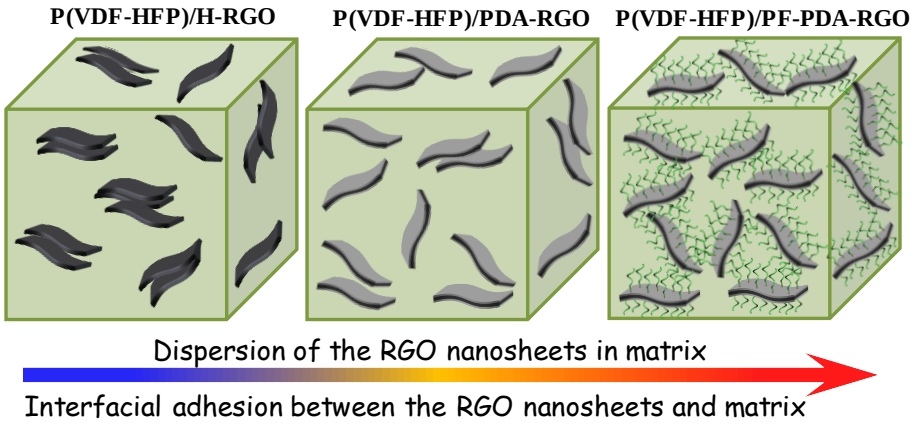

Fluoro-polymer functionalized graphene was synthesized as promising filler for flexible polymer-based nanodielectrics. The resulting nanocomposites exhibit high dielectric constant, suppressed dielectric loss and low percolation threshold.